Stacking-Fault Nucleation on Ir(111)

Carsten Busse,[1,*] Celia Polop,[1] Michael Müller,[2] Karsten Albe,[2] Udo Linke,[3] and Thomas Michely[1]
[1]*I. Physikalisches Institut, RWTH Aachen, D-52056 Aachen, Germany*
[2]*Fachbereich Material und Geowissenschaften, Technical University of Darmstadt, D-64289 Darmstadt, Germany*
[3]*ISG 3, Forschungszentrum Jülich, D-52425 Jülich, Germany*
(Received 9 April 2003; published 31 July 2003)

Variable temperature scanning tunneling microscopy experiments reveal that in Ir(111) homoepitaxy islands nucleate and grow both in the regular fcc stacking and in the faulted hcp stacking. Analysis of this effect in dependence on deposition temperature leads to an atomistic model of stacking-fault formation: The large, metastable stacking-fault islands grow by sufficiently fast addition of adatoms to small mobile adatom clusters which occupy in thermal equilibrium the hcp sites with a significant probability. Using parameters derived independently by field ion microscopy, the model accurately describes the results for Ir(111) and is expected to be valid also for other surfaces.

DOI: 10.1103/PhysRevLett.91.056103 PACS numbers: 68.35.Fx, 61.72.Nn, 68.37.Ef, 68.55.Jk

The morphology of a thin film as obtained by epitaxial growth can deviate from the perfect registry of the atoms given in a single crystal by the introduction of individual defects. One of the most important defects for the growth on fcc(111) is the stacking fault (SF), where atoms get trapped in hcp sites and areas of a metastable phase in an energetically disfavored stacking form. The two nonequivalent threefold hollow adsorption sites on fcc(111) are depicted in the ball model of Fig. 1(c). By occupying the fcc site a stacking sequence *ABc* is induced, whereas adsorption on an hcp site leads to *ABa*.

Growth in the presence of SFs leads to twin crystallite formation, which gets embedded in the regular matrix; incoherent twin boundaries evolve [1]. Therefore the density of SFs is decisive for the quality of thin films. On the other hand, an SF is not necessarily a "fault," and there are several systems where the energetically disfavored stacking shows desirable features. The most prominent example is the magnetic multilayer system Co/Cu(111), where fcc Co has superior magnetic properties. A lot of work has therefore been devoted to the problem of growing fcc Co layers on Cu(111) (e.g., [2–4]).

SF formation during homoepitaxy has been analyzed on several surfaces with a variety of methods. An early elegant study identifying SF islands by decoration with triangular islands was performed by Meinel *et al.* [5] for Ag/Ag(111) using transmission electron microscopy. Later, the different stacking types could be identified by low energy electron microscopy [6]. A study using x-ray scattering [7] implies that in this system the SFs nucleate heterogeneously, i.e., at defects or impurities of the original surface. Another example is Cu/Cu(111) where the temperature dependence of SF nucleation was studied using surface x-ray diffraction [8]. Here again heterogeneous nucleation was observed [9], and recently the formation of the SFs in this system was attributed to strain on the surface [10].

In summary, not even for the simplest case of SF formation, namely, homoepitaxy on a close-packed metal surface, can a concise picture of SF nucleation be extracted from the literature due to the problem of impurities, partly contradicting results, and an overall small variation of growth parameters be studied. Here, we present for the first time a kinetic model of stacking-fault nucleation, which quantitatively reproduces an extended data set for fault island probability in dependence of deposition temperature T and flux F. The model has no adjustment parameters and has as input data only the accurate field ion microscopy (FIM) data on Ir cluster diffusion on Ir(111) by Wang and Ehrlich [11–14]. The present study is therefore a powerful demonstration that mesoscopic growth phenomena may be quantitatively

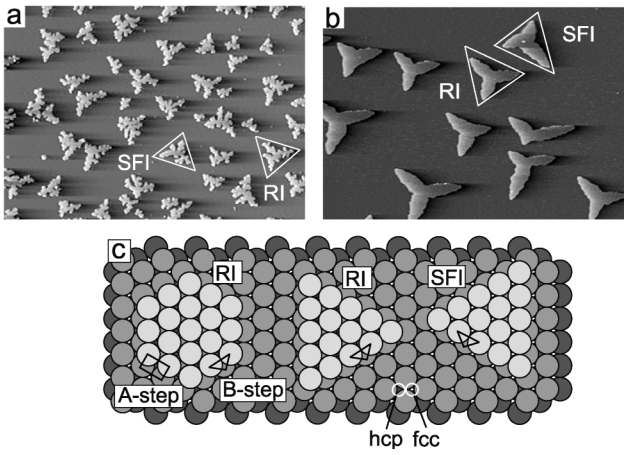

FIG. 1. (a),(b) STM topographs of stacking-fault islands after deposition of $\Theta = 0.13$ ML with $F = 1.3 \times 10^{-2}$ ML/s. (a) $T = 300$ K, scan width 1440 Å, $\frac{P_{\mathrm{SFI}}}{P_{\mathrm{RI}}} = 0.36 \pm 0.03$. (b) $T = 600$ K, scan width 2500 Å, $\frac{P_{\mathrm{SFI}}}{P_{\mathrm{RI}}} = 0.03 \pm 0.03$. In each picture a faulted (SFI) and a regular island (RI) are marked. (c) Ball model of an fcc(111) surface with (from left to right): hexagonal RI, note the difference between *A* and *B* steps, triangular RI bounded only by *B* steps, and triangular SFI with the same structure. Note the rotation by 180° between RI and SFI necessary to achieve equivalent step geometry.

understood on the basis of the present knowledge on atomistic processes.

The experiments were performed in an UHV chamber with a base pressure $P < 3 \times 10^{-11}$ mbar. The sample was cleaned by repeated cycles of sputtering and annealing, resulting in a clean surface and a terrace width of several 1000 Å. Prior to deposition the sample was flashed to a temperature ensuring desorption of all species that might have adsorbed from the background gas. Ir was evaporated with a standard deposition rate $F = 1.3 \times 10^{-2}$ ML/s from a resistance-heated wire. Special care was exercised to ensure clean deposition conditions ($P < 1 \times 10^{-10}$ mbar). After deposition the sample was quenched to avoid changes of island shapes. The resulting morphology was analyzed by variable temperature scanning tunneling microscopy (STM).

Two typical STM topographs showing SF formation are presented in Figs. 1(a) and 1(b). Under a wide range of temperature and flux conditions islands with a triangular envelope [indicated by the white triangles in Figs. 1(a) and 1(b)] grow on Ir(111). The growth kinetics enforcing this triangular island envelope bounded predominantly by B steps [compare Fig. 1(c)] may be traced back to an energetic preference of B steps on Ir(111) [15]. For a faulted island the requirement for a triangular island envelope bounded predominantly by B steps causes an apparent island rotation of 180°, allowing its straightforward identification. Atomically resolved images exhibiting adjacent faulted and unfaulted areas confirm the attribution of island rotation to stacking-fault occurrence.

Analyzing topographs like Figs. 1(a) and 1(b) yields the relative SFI (stacking-fault islands) probability $\frac{P_{\mathrm{SFI}}}{P_{\mathrm{RI}}} = \frac{\text{number of SFI}}{\text{number of RI}}$ with a temperature behavior as shown in Fig. 2. Below 230 K SFIs are even the majority species. Increasing T leads to a decrease of $\frac{P_{\mathrm{SFI}}}{P_{\mathrm{RI}}}$. For $T > 600$ K, no SFIs are observed.

An entire stacking-fault layer has an excess energy of about 0.08 eV/atom compared to a regular layer [16]. The large SFI formed are thus evidently metastable. We propose here a kinetic model for their formation based on small mobile clusters (Fig. 3): Without loss of generality, we assume to be in a temperature regime where monomers and dimers are mobile, but larger clusters are immobile at the time scale of the experiment [18]. Upon diffusion the dimers visit fcc and hcp sites alternatingly, so if the mobility of the dimers is sufficiently high (see below), we can assume the whole ensemble of dimers on the surface to be distributed among the inequivalent binding sites according to a Boltzmann distribution, i.e., the dimer ensemble is in thermal equilibrium. Since the energy difference between these sites is small (see Table I), a significant fraction of dimers will occupy hcp sites. With the addition of one more adatom a dimer becomes immobile at the temperature under concern, so the distribution of trimers reflects the equilibrium distribution of the dimers over the two possible sites. All successively incoming adatoms thus have to adopt the present stacking sequence, until finally large islands evolve which are metastable only in the disfavored hcp stacking. Of course, for higher temperatures also larger clusters will become mobile, and then the equilibrium distribution of the largest mobile cluster will govern the distribution of the islands.

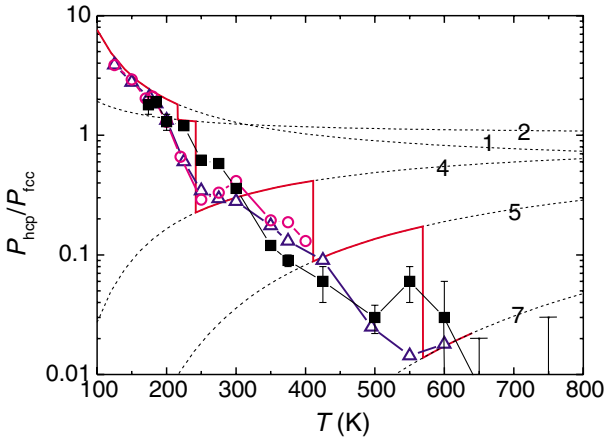

FIG. 2 (color online). Temperature dependence of relative stacking-fault probability $\frac{P_{\mathrm{SFI}}}{P_{\mathrm{RI}}}$ as measured in experiment (■); full line: atomistic model of the effect; open triangles (△): solution of rate equations; open circles (○): kinetic Monte Carlo simulation, both using parameters derived by FIM; dashed lines: equilibrium distributions of small clusters (see labels) extrapolated from FIM measurements; see Table I. See text.

The model described above can be generalized as follows: A cluster of size i is considered as mobile if the time τ_i it needs to interchange between fcc and hcp is smaller than the time τ_{+1} needed to add an additional atom to it: $\tau_i < \tau_{+1}$. For a first approximation of τ_i it is sufficient to look at the slower process of jumps from hcp to fcc and vice versa. Since this process is then also the rate-limiting step in overall cluster diffusion, one can approximate

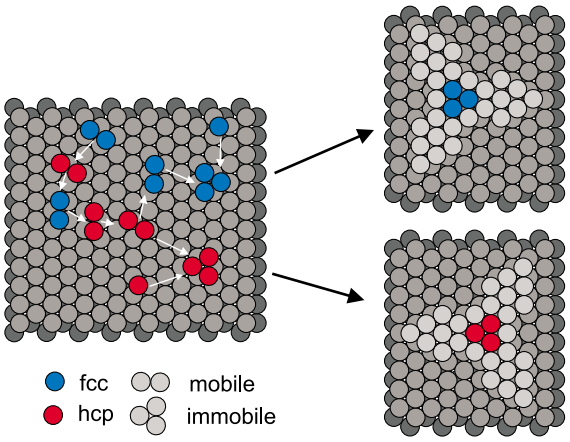

FIG. 3 (color online). Atomistic model of stacking-fault nucleation.

TABLE I. Results for different cluster sizes: Cluster size i, observed stacking-fault probability $\frac{P_{\mathrm{hcp}}}{P_{\mathrm{fcc}}}$ at temperature T_m, differences in energy $\Delta E_{b,i}$, entropy $\Delta S_{b,i}$, and free energy ΔF_i at T_m; effective diffusion barrier $E_{d,i}$ and effective prefactor of diffusion $D_{0,i}$ (all from FIM), transition temperature $T_{t,i}$ for which $i^\dagger = i$; $(*)$ highest point in temperature sequence; $(\dagger)$ extrapolated from $\Delta E_{b,i<5}$ by assuming $\frac{\Delta E_{b,i}}{i}$ to approach the value for 1 ML (-0.081 eV/atom [16]) exponentially, using $\Delta E_{b,i} \approx \Delta F_i$ where $\Delta E_{b,i}$ is not known. Parameters from [14] corrected according to an improved temperature calibration [12] (see also [17]).

i	$\frac{P_{\mathrm{hcp}}}{P_{\mathrm{fcc}}}$	T_m (K)	$\Delta E_{b,i}$ (eV)	$\Delta S_{b,i}$ (k_B)	$\Delta F_i(T_m)$ (eV)	$E_{d,i}$ (eV)	$D_{0,i}$ ($\frac{\mathrm{cm}^2}{\mathrm{s}}$)	$T_{t,i}$ (K)
1	5.7* [11]	106* [11]	0.023 [11,12]	0.64 [11]	0.017	0.290 ± 0.003 [13]	$3.8 \times 1.4^{\pm 1} \times 10^{-4}$ [13]	
2	1.5 [14]	160 [14]			0.0056	0.447 ± 0.013 [12,14]	$2.6 \times 2.2^{\pm 1} \times 10^{-5}$ [12,14]	216
3	1 [14]	250 [14]			0	0.646 ± 0.018 [12,14]	$4.2 \times 2.4^{\pm 1} \times 10^{-4}$ [12,14]	299
4	0.176 [14]	205 [14]			-0.031	0.477 ± 0.014 [12,14]	$1.5 \times 2.3^{\pm 1} \times 10^{-5}$ [14]	242
5			$-0.086^\dagger$			0.685 ± 0.016 [12,14]	$6.0 \times 1.9^{\pm 1} \times 10^{-6}$ [12,14]	411
6			$-0.15^\dagger$			≈ 0.93 [14]	$\approx 10^{-5}$ [14]	592
7			$-0.21^\dagger$			1.49 ± 0.03 [13]	$1.4 \times 2.4^{\pm 1}$ [13]	569

$\tau_i \approx \frac{a^2}{4D_i}$, with D_i the diffusion coefficient of a cluster of size i and a the nearest-neighbor distance. D_i were measured by FIM and approximated by

$$D_i = D_{0,i} e^{-E_{d,i}/k_B T}, \tag{1}$$

with $D_{0,i}$ the prefactor for diffusion and $E_{d,i}$ the effective energy barrier (see Table I).

An approximation of τ_{+1} is $\tau_{+1} = \frac{n_{\mathrm{sat}}}{F}$, i.e., the time between two successive deposition events into the capture area of the cluster, assuming the cluster density to be given by the experimental saturation island density n_{sat} [19].

Now we can apply the mobility criterion $\tau_i < \tau_{+1}$ to distinguish between mobile clusters with a size $i \leq i^\dagger$, i.e., $i^\dagger$ being the largest mobile cluster, and immobile clusters with $i > i^\dagger$. With increasing temperature τ_{+1} decreases slower than τ_i, so we can define a transition temperature $T_{t,i}$ at which mobility sets in by demanding $\tau_{+1} = \tau_i$ [see Table I, note that the tetramer (heptamer) becomes mobile earlier than the trimer (hexamer), thus playing a minor role in the nucleation of the SFs].

Mobile clusters by definition diffuse efficiently, and are thus distributed between the inequivalent binding sites according to a Boltzmann distribution

$$\left(\frac{P_{\mathrm{hcp}}}{P_{\mathrm{fcc}}}\right)_i = e^{\Delta F_{b,i}/k_B T}, \tag{2}$$

with $\Delta F_i = F_{i,\mathrm{fcc}} - F_{i,\mathrm{hcp}}$ being the difference in free energy. ΔF_i is obtained by $\Delta F_i(T) = \Delta E_{b,i} - T\Delta S_i$ for $i = 1$ [$\Delta E_{b,i}$ (ΔS_i) the difference in binding energy (entropy)], $\Delta F_i(T) \approx \Delta F_i(T_m)$ (with T_m the temperature of the FIM experiment) for $1 < i \leq 4$, and $\Delta F_i(T) \approx \Delta E_{b,i}$ for $i > 4$ (see Table I).

At each temperature the distribution of the large islands (compare Fig. 1) is therefore given by the equilibrium distribution of the largest mobile cluster $i^\dagger$ at this temperature: $\frac{P_{\mathrm{SFI}}}{P_{\mathrm{RI}}} = (\frac{P_{\mathrm{hcp}}}{P_{\mathrm{fcc}}})_{i^\dagger}$. In this model we therefore expect the T dependence of $\frac{P_{\mathrm{SFI}}}{P_{\mathrm{RI}}}$ to be given by segments of Boltzmann distributions for increasing $i^\dagger$ connected by jumps at the respective $T_{t,i}$.

This model with the values from Table I is superimposed on our data in Fig. 2 (full line). It is visible that the simple atomistic picture describes the overall behavior of the data without using any adjustable parameters and thus seems to capture the relevant physical effects responsible for the SF nucleation. Note that $\Delta E_{b,i}$ for pentamers and heptamers is obtained by extrapolating the FIM values for smaller entities.

We have gone beyond this simple and instructive atomistic model by a mean-field approach taking into account the presence of two different adsorption sites ($s = f, h$), thus extending the well-established rate equations of island nucleation [20,21], defining n_1^s as the density of clusters of size i in the respective stacking s. As an example, the time variation of adatoms in fcc stacking n_1^{f} is given by

$$\begin{aligned}\frac{dn_1^f}{dt} = {} & \frac{F(1-\Theta)}{2} - 2D_1^f n_1^f \sigma_1 n_1^f - D_1^f n_1^f \sigma_1 n_1^h \\ & - D_1^f n_1^f \sum_{s=f,h} \sum_{m=2}^{8} \sigma_m n_m^s + \sum_{s=f,h} \Gamma_2^s n_2^s - n_1^f \nu_1^f \\ & + n_1^h \nu_1^h. \end{aligned} \tag{3}$$

The terms on the right-hand side describe deposition of atoms (taking into account that landing atoms find two kinds of sites on the surface), association of an fcc dimer, association of two fcc monomers, association of an fcc with an hcp monomer, attachment of fcc adatoms to larger clusters (assuming they take over the stacking of these entities), dissociation of dimers (assuming this process to yield with equal probability two fcc or two hcp monomers), and hopping of adatoms between fcc and hcp sites. The last two terms are the most important extension of the established approach, as they allow exchange between the different species on the surface. The equations for larger clusters can be obtained in the same way; the complete set of equations will be described in a

forthcoming publication. We derive the diffusion coefficient D_1^s of atoms in the respective stacking by treating them as two independent species. For monomers, the necessary parameters were derived explicitly [22]. $D_{i>1}^s$ is obtained from Eq. (1) with taking the values from Table I for the high barrier process and using a modified $\tilde{E}_{d,i} = E_{d,i} - |\Delta F_i|$ for the low barrier process [23]. For the capture number σ_i we set $\sigma_i = 3$ for $i < 8$ and $\sigma_i = 7$ for $i \geq 8$ [20]. The dissociation rate for dimers Γ_2^s is calculated using $E_{\mathrm{diss},2}^f = 1.15\,\mathrm{eV}$, $E_{\mathrm{diss},2}^h = 1.17\,\mathrm{eV}$ [19], and $\nu_{0,\mathrm{diss}} = k_B T/h$. Dissociation of larger clusters than dimers is negligible.

Taking $n_x^s = \sum_{i>7} n_i^s$ we integrated the total set of 16 differential equations numerically to yield $\frac{P_{\mathrm{SFI}}}{P_{\mathrm{RI}}}$. The resulting curve is in excellent agreement with the measurements (see Fig. 2), smoothing the unphysical, sharp transitions of the simple model. A test of this rate-equation approach was performed by comparing the total saturation island density obtained with the values derived from the STM measurements [19]; also here the solution is in excellent agreement with the measured values.

In addition to the temperature dependent measurements described in detail, we have also studied the defect formation in dependence on deposition rate. The observed increase of probability for metastable faulted island nucleation with increasing rate is reproduced by the rate equations. This finding offers a possible explanation for suppression of the equilibrium structure of a Co film on Cu(111) up to higher film thickness if the method of pulsed laser deposition is employed which involves an extremely high deposition rate.

Furthermore, we also performed kinetic Monte Carlo simulations of the homoepitaxial growth of Ir on Ir(111). The simulations were carried out on a refined lattice containing fcc as well as hcp sites. Atoms were deposited onto the surface at random sites with a deposition rate of 1.3×10^{-2} ML/s. The surface area measured 1000×1000 Å^2 for simulated temperatures below 325 K. For higher temperatures, the area had to be increased to 1500×1500 Å^2 in order to achieve a sufficient number of islands. The Monte Carlo code identified clusters on the Ir surface up to $i = 5$, the diffusion of these clusters was simulated by allowing them to jump from an fcc-binding site to an hcp-binding site and vice versa. The parameters $\nu_{0,i}$ and $E_{d,i}$ determining the rates for these transitions were the same as used in the rate equations described above. The results of these simulations are also presented in Fig. 2; their accordance with the experimental results is obvious.

In conclusion, we have observed stacking-fault islands on Ir(111) and traced their formation back to the underlying atomic mechanism: The equilibrium distribution of small clusters between hcp and fcc is frozen in by the attachment of immobilizing adatoms during growth. A simple atomistic model already describes the effect quantitatively. Full agreement with the experiment can be achieved by solving rate equations using parameters derived independently by FIM. The model should also hold for other fcc(111) surfaces.

We acknowledge the experimental help of A. Petersen and communication of the recalibrated Ir cluster diffusion parameters by G. Ehrlich. This work was supported by the Deutsche Forschungsgemeinschaft via the project "Atomare Prozesse beim homoepitaktischen Schichtwachstum unter extremen Nichtgleichgewichtsbedingungen."

*Corresponding author.
Email address: busse@physik.rwth-aachen.de

[1] M. J. Stowell, *Epitaxial Growth* (Academic Press, New York, San Francisco, London, 1975), Pt. B.
[2] M. Zheng *et al.*, Appl. Phys. Lett. **74**, 425 (1999).
[3] P. LeFevre, H. Magnan, O. Heckmann, V. Briois, and D. Chandesris, Phys. Rev. B **52**, 11 462 (1995).
[4] J. Camarero *et al.*, Phys. Rev. Lett. **73**, 2448 (1994).
[5] K. Meinel, M. Klaua, and H. Bethge, Phys. Status Solidi A **110**, 189 (1988).
[6] J. Tersoff, A.W. Denier van der Gon, and R. M. Tromp, Phys. Rev. Lett. **72**, 266 (1994).
[7] S. A. de Vries *et al.*, Phys. Rev. Lett. **81**, 381 (1998).
[8] J. Camarero *et al.*, Surf. Sci. **459**, 191 (2000).
[9] H. A. van der Vegt, J. Alvarez, X. Torrelles, S. Ferrer, and E. Vlieg, Phys. Rev. B **52**, 17 443 (1995).
[10] M. Giesen and H. Ibach, Surf. Sci. **529**, 135 (2003).
[11] S. C. Wang and G. Ehrlich, Phys. Rev. Lett. **68**, 1160 (1992).
[12] G. Ehrlich (private communication).
[13] S. C. Wang, U. Kürpick, and G. Ehrlich, Phys. Rev. Lett. **81**, 4923 (1998).
[14] S. C. Wang and G. Ehrlich, Surf. Sci. **239**, 301 (1990).
[15] M. J. Rost, T. Michely, and G. Comsa, Phys. Rev. B **57**, 1992 (1998).
[16] J. C. Hamilton, M. R. Sorensen, and A. F. Voter, Phys. Rev. B **61**, R5125 (2000).
[17] K. Kyuno, A. Gölzhäuser, and G. Ehrlich, Surf. Sci. **397**, 191 (1998).
[18] As a first approximation one can assume the mobility of clusters to decrease with increasing size, see, e.g., [14].
[19] C. Busse *et al.*, Surf. Sci. Lett. **539**, L560 (2003).
[20] J. A. Venables, Philos. Mag. **27**, 697 (1973).
[21] J. A. Venables, G. D. T. Spiller, and M. Hanbücken, Rep. Prog. Phys. **47**, 399 (1984).
[22] We use $\nu_1^s = \nu_{0,1}^s e^{-E_{d,1}^s/k_{BT}}$ and $D_1^s = \frac{1}{4}\nu_1^s a_{nn}^2$ with the values from [11] modified according to [12]: $E_{d,1}^f = (0.270 \pm 0.003)\,\mathrm{eV}$, $E_{d,1}^h = (0.293 \pm 0.003)\,\mathrm{eV}$, $\nu_{0,1}^f = 8.1 \times 1.4^{\pm 1} \times 10^{11}\,\mathrm{Hz}$, and $\nu_{0,1}^h = 1.7 \times 1.4^{\pm 1} \times 10^{12}\,\mathrm{Hz}$.
[23] Using an exact formula for diffusion on inequivalent binding sites only marginally influences the resulting curve.